Electron-Transfer and Acid−Base Properties of a Two-Electron Oxidized Form of Quaterpyrrole that Acts as Both an Electron Donor and an Acceptor

Min Zhang,[†] Wenbo E,[†] Kei Ohkubo,[‡] David Sanchez-Garcia,[§] Dae-Wi Yoon,[§] Jonathan L. Sessler,*[,§] Shunichi Fukuzumi,*[,‡] and Karl M. Kadish*[,†]

Department of Chemistry, University of Houston, Houston, Texas 77204-5003, Department of Material and Life Science, Graduate School of Engineering, Osaka University, SORST, Japan Science and Technology Agency (JST), Suita, Osaka 565-0871, Japan, and Department of Chemistry & Biochemistry, University Station-A5300, The University of Texas, Austin, Texas 78712-0165

Received: August 17, 2007

Electron-transfer interconversion between the four-electron oxidized form of a quaterpyrrole (abbreviated as **P_4** for four pyrroles) and the two-electron oxidized form (**P_4H_2**) as well as between **P_4H_2** and its fully reduced form (**P_4H_4**) bearing analogous substituents in the α- and *β*-pyrrolic positions was studied by means of cyclic voltammetry and UV−visible spectroelectrochemistry combined with ESR and laser flash photolysis measurements. The two-electron oxidized form, **P_4H_2**, acts as both an electron donor and an electron acceptor. The radical cation (**$P_4H_2^{\bullet+}$**) and radical anion (**$P_4H_2^{\bullet-}$**) are both produced by photoinduced electron transfer from dimeric 1-benzyl-1,4-dihydronicotinamide to **P_4H_2**, whereas the cation radical form of the compound is also produced by electron-transfer oxidation of **P_4H_2** with $[Ru(bpy)_3]^{3+}$. The ESR spectra of **$P_4H_2^{\bullet+}$** and **$P_4H_2^{\bullet-}$** were recorded at low temperature and exhibit spin delocalization over all four pyrrole units. Thus, the two-electron oxidized form of the quaterpyrrole (**P_4H_2**) displays redox and electronic features analogous to those seen in the case of porphyrins and may be considered as a simple, open-chain model of this well-studied tetrapyrrolic macrocycle. The dynamics of deprotonation from **$P_4H_2^{\bullet+}$** and disproportionation of **P_4H_2** were examined by laser flash photolysis measurements of photoinduced electron-transfer oxidation and reduction of **P_4H_2**, respectively.

Introduction

Open-chain oligopyrroles have attracted increasing attention recently as potential building blocks for new types of porphyrins and related macrocycles, as well as for applications running the gamut from materials science to drug development.[1−7] Among the various known systems, *β*-substituted, α-linked oligomers are of particular interest because the *β*-pyrrolic substituents provide the solubility necessary for both initial characterization and subsequent manipulation and use. However, until recently, relatively elaborate multistep syntheses were required to obtain higher order open-chain oligopyrroles (i.e., α-linked oligomers containing more than three pyrroles). This has limited their application in synthesis and has precluded detailed investigations of their electronic, electrochemical, and spectroscopic properties and hence fundamental comparisons to porphyrins and other well-studied tetrapyrrolic macrocycles to which they might be expected to bear analogy.[8−15] Recently, however, we have developed improved syntheses of *β*-substituted quaterpyrroles (abbreviated as **P_4H_2** for four pyrroles and two protons) that involve the oxidative homocoupling of bipyrrole.[16,17] The initial **P_4H_2** product of this coupling is the two-electron oxidized form of the quaterpyrrole, which is a relatively stable species that may easily be reduced chemically or electrochemically to provide the less-stable fully reduced form of the pyrrole represented as **P_4H_4**.

We have also applied the enolate coupling, 1,4-dicarbonyl cyclization method to obtain odd-numbered oligopyrroles.[16] This made it feasible to explore the electron-transfer properties of the fully reduced bi-, ter-, and quaterpyrroles (**P_2H_2**, **P_3H_3**, and **P_4H_4**, respectively) bearing analogous substituents in the α- and *β*-pyrrolic positions. This was done in a recent publication where we analyzed redox potentials and effective conjugation pathways as a function of subunit number and chain length by means of cyclic voltammetry, ESR and UV−vis spectroelectrochemistry.[17]

A comparison of $E_{1/2}$ values for the first one-electron abstraction from the bipyrrole **P_2H_2** (1.07 V), terpyrrole **P_3H_3** (0.67 V), and quaterpyrrole **P_4H_4** (0.44 V) revealed that the longer oligopyrroles are easier to oxidize, as would be expected given the potentially longer conjugation pathways that such systems can provide.[17] In the context of this study, we found that **P_4H_4** could be oxidized by two electrons and two protons to generate **P_4H_2**, with the corresponding one electron intermediate, **$P_4H_4^{\bullet+}$**, being characterized by UV−visible spectroelectrochemistry in CH_2Cl_2.[17]

The chemical reduction[16] of **P_4H_2** to **P_4H_4** and its electrochemical oxidation[13] back to **P_4H_2** is similar to the two-proton tranformations that accompany the electrochemical reduction of porphyrins.[18] This led us to consider that **P_4H_2** might serve as an open-chain, electronic model for porphyrins. To explore this analogy more fully, we have now carried out a detailed analysis of the two-electron reduction (**P_4H_2**−**P_4H_4**) as well as two-electon oxidation (**P_4H_2**−**P_4**) processes using cyclic voltammetry, thin-layer spectroelectrochemistry, and ESR spec-

* Corresponding authors. K.M.K.: fax, (713) 743-2745; tel, (713) 743-2741; e-mail, kkadish@uh.edu. S.F.,: e-mail, fukuzumi@chem.eng.osaka-u.ac.jp. J.L.S.: fax, 1 512 471 7550; tel, 1 512 471 5009; e-mail: sessler@mail.utexas.edu.

[†] University of Houston.

[‡] Osaka University and JST.

[§] The University of Texas.

10.1021/jp0766306 CCC: $40.75
Published on Web 01/25/2008

SCHEME 1

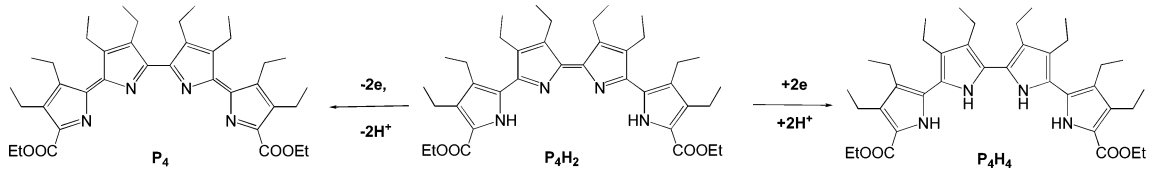

troscopy. We have found that electrochemical conditions under which the initial two-electron oxidized form of the quaterpyrrole ($\mathbf{P_4H_2}$) could be converted into its fully oxidized $\mathbf{P_4}$ form or its fully reduced form $\mathbf{P_4H_4}$ (cf. Scheme 1 for overall two-electron transfer and protonation/deprotonation reactions). We have also examined the dynamics of deprotonation from $\mathbf{P_4H_2}^{\bullet+}$ and disproportionation of $\mathbf{P_4H_2}^{\bullet-}$ by laser flash photolysis measurements of photoinduced electron-transfer oxidation and reduction of $\mathbf{P_4H_2}$, respectively. In both cases, the relevant one-election intermediates could be characterized at several different protonation states. Thus, this study provides the full characterization of redox and acid−base intermediates in redox reactions of the open-chain quaterpyrrole (Scheme 1).

Experimental Section

Chemicals. Anhydrous dichloromethane (CH_2Cl_2) was purchased from EMD Chemical Co. and used as received without further purification. Tetra-*n*-butylammonium perchlorate (TBAP) was purchased from Sigma Chemical or Fluka Chemika Co., recrystallized from ethyl alcohol, and dried under vacuum at 40 °C for at least 1 week prior to use. Trifluroacetic acid (TFA) was purchased from Fluka Chemika Co. Tetra-*n*-butylammonium hydroxide (TBAOH) was purchased from Sigma-Aldrich Chemical Co. 9-Mesityl-10-methylacridinium perchlorate ($[Acr^+-Mes]ClO_4^-$) was purchased from Tokyo Chemical Industry (TCI) Co., Ltd. The dimeric 1-benzyl-1,4-dihydronicotinamide, $(BNA)_2$, was prepared according to the literature.[19,20] The oxidized and reduced forms of quaterpyrrole were prepared as described previously.[17]

Instrumentation. Cyclic voltammetry was carried out with an EG&G Princeton Applied Research (PAR) 173 potetiostat/galvanostat. A homemade three-electrode cell was used for cyclic voltammetric measurements and consisted of a platinum button or glassy carbon working electrode, a platinum counter electrode, and a homemade saturated calomel reference electrode (SCE). The SCE electrode was separated from the bulk of the solution by a fritted glass bridge of low porosity, which contained the solvents/supporting electrolyte mixture. UV−visible spectroelectrochemical experiments were performed with a home-built thin-layer cell[21] that had a light transparent platinum net working electrode. Potentials were applied and monitored with an EG&G PAR Model 173 potentiostat. Time-resolved UV−visible spectra were recorded with a Hewlett-Packard Model 8453 diode array spectrophotometer. The ESR measurements were performed on a JEOL JES-FA100 ESR spectrometer. The ESR spectra were recorded under nonsaturating microwave power conditions. The magnitude of modulation was chosen to optimize the resolution and the signal-to-noise (S/N) ratio of the observed spectra. The *g* value and hyperfine coupling constants (hfc) were calibrated by using an Mn^{2+} marker.

Laser Flash Photolysis Measurements. Measurements of transient absorption spectra in the photochemical reactions of $\mathbf{P_4H_2}$ with $(BNA)_2$ and Acr^+-Mes were performed according to the following procedure: A degassed CH_3CN_3 solution containing Acr^+-Mes or $(BNA)_2$ and $\mathbf{P_4H_2}$ was excited by a Nd:YAG laser (Continuum, SLII-10, 4−6 ns fwhm) at 355 nm. The resulting time-resolved transient absorption spectra were then measured by using a continuous Xe-lamp (150 W) and a photodiode (Hamamatsu 2949) as the probe light and detector, respectively. The output from the photodiode and the photomultiplier tube was recorded using a digitizing oscilloscope (Tektronix, TDS3032, 300 MHz).

Theoretical Calculations. Density functional calculations were performed with Gaussian03 (Revision C.02, Gaussian, Inc.)[22] using the spin-restricted B3LYP functional for the open-shell molecule on an eight-processor QuantumCube developed by Parallel Quantum Solutions.[23]

Results and Discussion

Electrochemistry and Spectroelectrochemistry in CH_2Cl_2. The two-electron oxidized form of the quaterpyrrole, $\mathbf{P_4H_2}$, undergoes two irreversible oxidations and three reductions in CH_2Cl_2, the first two of which are also irreversible, as illustrated in Figure 1. Similar current−voltage curves and peak potentials were obtained by regular and thin-layer cyclic voltammetry (CV). The irreversible nature of the first oxidation and first reduction processes are consistent with the products of these electron-transfer reactions being unstable on the cyclic voltammetry time scale. However, as will be shown in the following section, the singly oxidized and singly reduced forms of $\mathbf{P_4H_2}$ could both be characterized by ESR spectroscopy after being produced *in situ* using chemical means. In addition, it was found that many of the electron-transfer steps of $\mathbf{P_4H_2}$ are coupled with protonation events.

Nonetheless, the global processes involving the addition or abstraction of electrons and protons were in all cases reversible under the application of an appropriate oxidizing or reducing potential. On this basis, we conclude that little or no decomposition of the quaterpyrrole occurred under the electrochemical conditions and that, as a consequence, such methods could be used to probe the interconversions between $\mathbf{P_4H_2}$ and $\mathbf{P_4H_4}$ or $\mathbf{P_4}$.

To evaluate the prevailing electron-transfer mechanisms in CH_2Cl_2, the products of each oxidation and reduction were

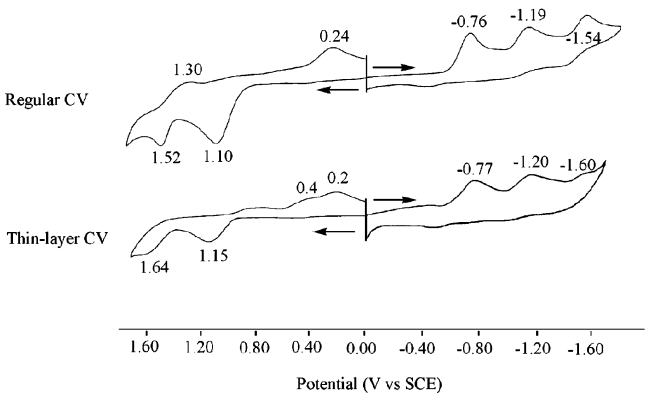

Figure 1. Regular and thin-layer cyclic voltammograms of the two-electron oxidized form of the quaterpyrrole, $\mathbf{P_4H_2}$, in CH_2Cl_2 containing 0.1 M TBAP.

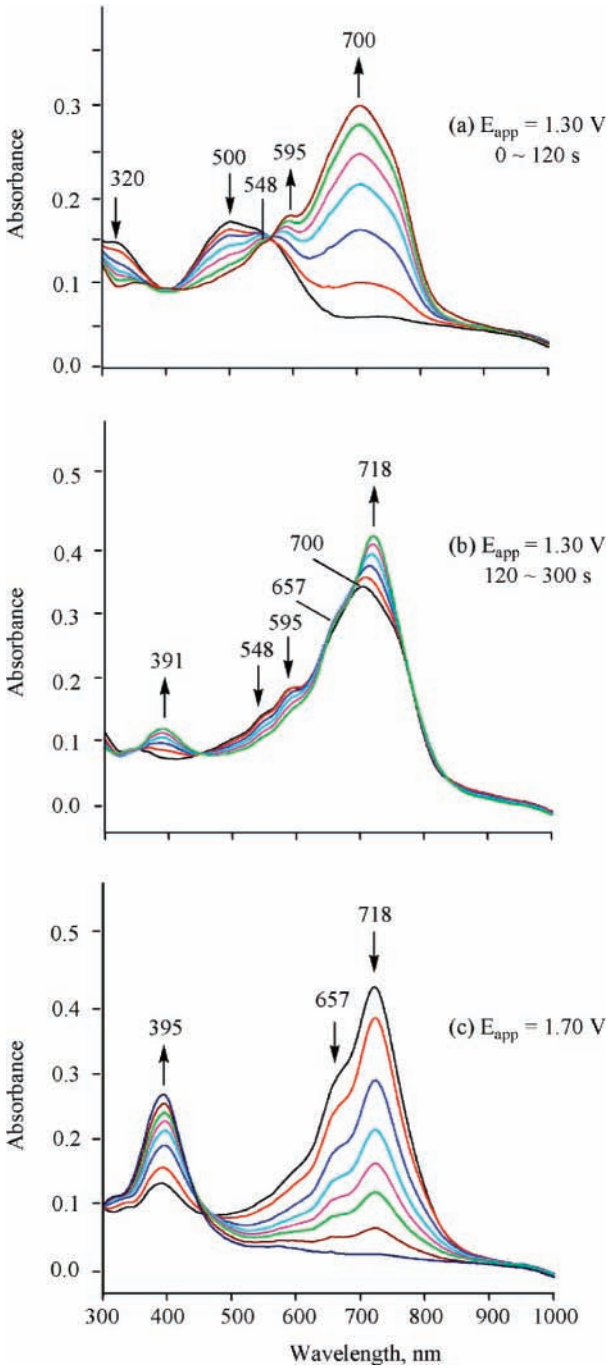

Figure 2. UV−visible spectral changes observed during the first and second electrochemical oxidations of $\mathbf{P_4H_2}$ in CH_2Cl_2 containing 0.2 M TBAP.

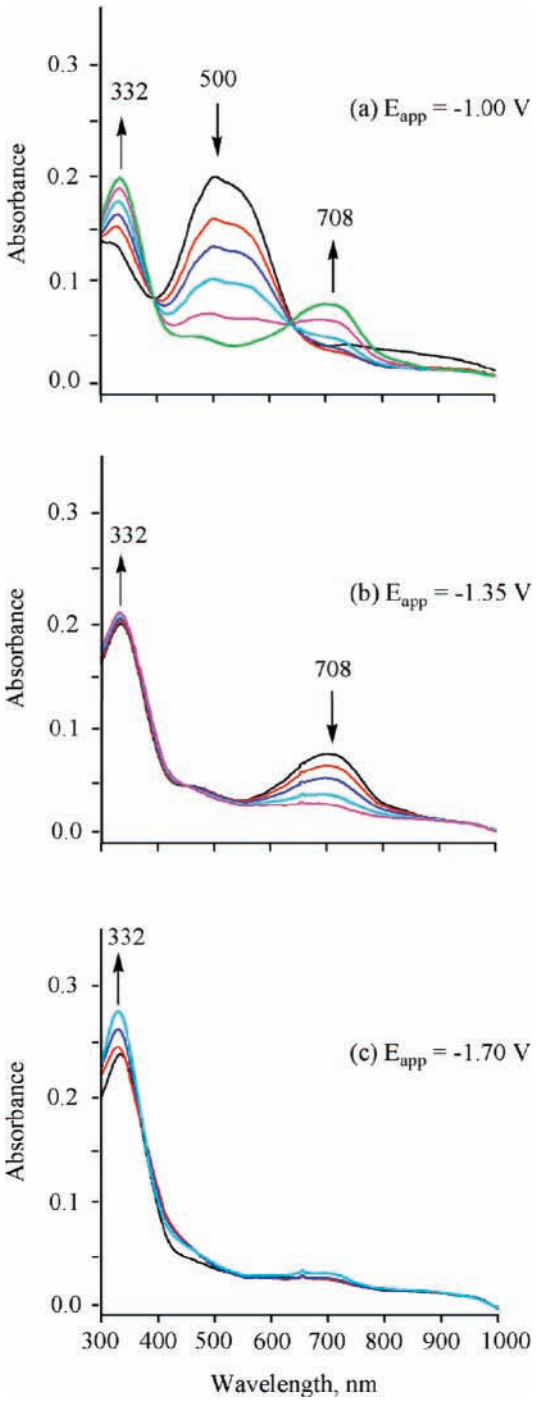

Figure 3. UV−visible spectral changes observed during the three electrochemical reductions of $\mathbf{P_4H_2}$ in CH_2Cl_2 containing 0.2 M TBAP.

monitored by thin-layer spectroelectrochemistry; examples of the resulting UV−visible spectra are shown in Figure 2 for electrooxidation at the indicated applied potentials.

Two sequential sets of spectral changes, each with isosbestic points, are obtained upon applying a controlled oxidizing potential of +1.30 V. The first set of changes (Figure 2a) occurs from 0 to 120 s after application of the oxidizing potential and is characterized by a decrease in intensity of the 500 nm band for neutral $\mathbf{P_4H_2}$ and the appearance of a new UV−visible spectrum with a strong absorption at 700 nm, a shoulder at 760 nm and two smaller bands at 548 and 595 nm. There is also a well-defined isosbestic point at 563 nm. The appearance of this spectrum is then followed by a second set of spectral changes that occur from 120−300 s after application of the potential as shown in Figure 2b. Again, isosbestic behavior is observed. The final oxidation product is generated at +1.70 V and is assigned to $\mathbf{P_4}$, a species that is characterized by a single band at 395 nm and no other absorption features between 300 and 1000 nm. This spectrum is shown in Figure 2c.

The electrochemical conversion of $\mathbf{P_4H_2}$ to $\mathbf{P_4H_4}$ was also monitored by thin-layer spectroelectrochemistry in CH_2Cl_2 during controlled potential reduction at of −1.00, −1.35, and −1.70 V, each value representing the potential position of the irreversible reduction peaks shown in Figure 1. These spectral changes are illustrated in Figure 3.

As seen in Figure 3a, controlled potential reduction of $\mathbf{P_4H_2}$ at −1.00 V leads to a disappearance of the characteristic broad band centered at around 500 nm,[17] and the appearance of two

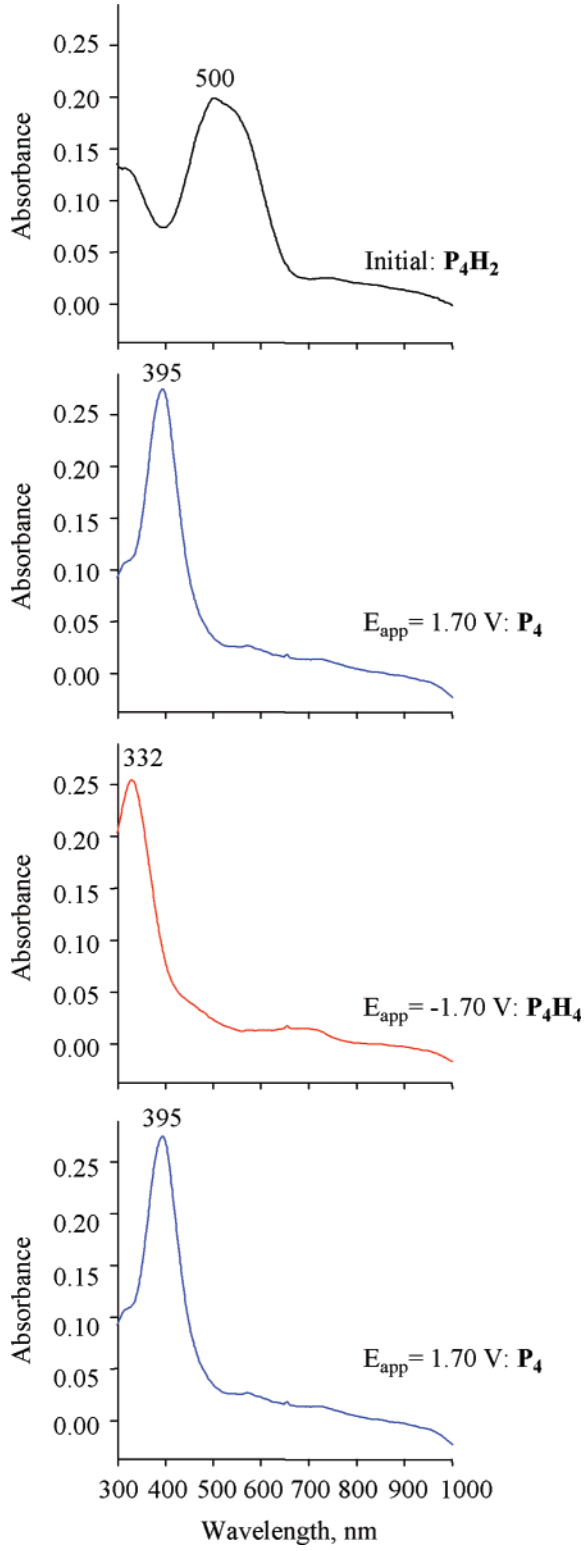

Figure 4. Key spectroscopic features associated with the proposed conversion between $\mathbf{P_4H_2}$, $\mathbf{P_4}$, and $\mathbf{P_4H_4}$ in CH_2Cl_2 containing 0.2 M TBAP.

new bands at 332 and 708 nm. Isosbestic points are observed at 394 and 640 nm, a finding we interpret in terms of a rapid equilibrium between two forms of the quaterpyrrole in solution. When a potential of −1.35 V is applied, the band at 708 nm decreases in intensity and the band at 332 nm increases slightly (Figure 3b). Moving the potential to −1.70 V (Figure 3c) leads to a further increase in intensity of the 332 nm band. This is the only band remaining at the end of the electrolysis and is

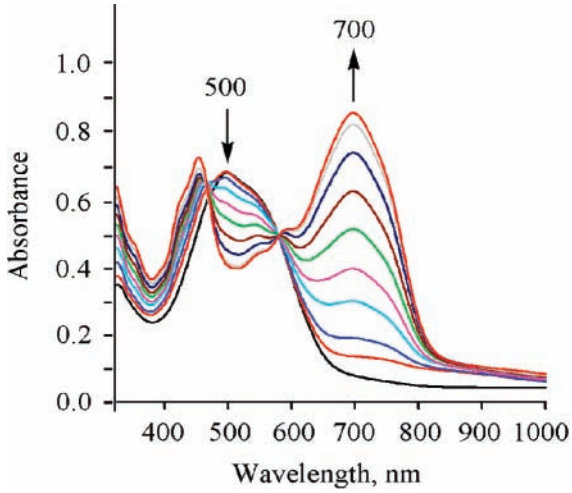

Figure 5. Spectral changes observed during the chemical one-electron oxidation of 1.66×10^{-4} M $\mathbf{P_4H_2}$ with $[Ru(bpy)_3]^{3+}$ in CH_2Cl_2. The final spectrum was obtained after the addition of 1 equiv of $[Ru(bpy)_3]^{3+}$.

assigned to $\mathbf{P_4H_4}$. Thus the overall spectral changes in Figures 2 and 3 are consistent with conversion of $\mathbf{P_4H_2}$ to $\mathbf{P_4}$ upon abstraction of two electrons and two protons and the conversion of $\mathbf{P_4H_2}$ to $\mathbf{P_4H_4}$ upon addition of two electrons and two protons, as shown in Scheme 1.

The electrochemically induced conversions between $\mathbf{P_4H_2}$ and $\mathbf{P_4H_4}$ or $\mathbf{P_4}$ lead us to suggest that the "reverse" processes, involving reduction of $\mathbf{P_4}$ and oxidation of $\mathbf{P_4H_4}$ might also be possible by application of an appropriate reducing or oxidizing potential. This was indeed the case as inferred from monitoring the UV−visible spectra as the potential in the thin-layer cell was sequentially set at first +1.70 V and then −1.70 V, and then taken back to +1.70 V again. The final spectra obtained at each potential at the end of each respective electrolysis step are shown in Figure 4. Conversion between the totally protonated and totally deprotonated forms of the quaterpyrrole was carried out at least five times with no apparent loss of intensity in the absorption bands. Of some significance is the fact that conversion of $\mathbf{P_4H_4}$ to $\mathbf{P_4}$ invariability passed through $\mathbf{P_4H_2}$, as indicated by the appearance of a transient spectrum for this species. However, this was not the case for conversion of $\mathbf{P_4}$ to $\mathbf{P_4H_4}$, a process that revealed no evidence for $\mathbf{P_4H_2}$ as an intermediate. Thus, the prevailing mechanism is considered to be that given in Scheme 2.

Chemical One-Electron Oxidation of $\mathbf{P_4H_2}$ in CH_2Cl_2. A chemical one-electron oxidation of $\mathbf{P_4H_2}$ by $[Ru(bpy)_3]^{3+}$ in CH_2Cl_2 gives spectral changes similar to those obtained during the initial electrochemical oxidation of $\mathbf{P_4H_2}$ (Figure 2a); these spectra are shown in Figure 5. After adding 1 equiv of oxidizing agent to solution, the spectrum is characterized by a major band at 700 nm, a shoulder at 750 nm and two smaller bands at 542 and 587 nm. These absorptions can be compared to bands at 700, 760 sh, 548, and 595 nm seen for the first one-electron oxidized product in the thin-layer cell. There is also an additional band at 453 nm seen in the spectrum of the chemically oxidized form of quaterpyrrole presented in Figure 5. This band, which is not due to the quaterpyrrole, is assigned to $[Ru(bpy)_3]^{2+}$.

Protonation and Spectroelectrochemisty of $\mathbf{P_4H_2}$ in CH_2Cl_2. The two-electron oxidized form of $\mathbf{P_4H_2}$ was subject to titration with trifluoroacetic acid (TFA) in CH_2Cl_2; this was done in an effort to probe the effect of protonation. The relevant spectral changes are shown in Figure 6. After addition of 100 equiv of TFA, the final spectrum is similar to that obtained during the

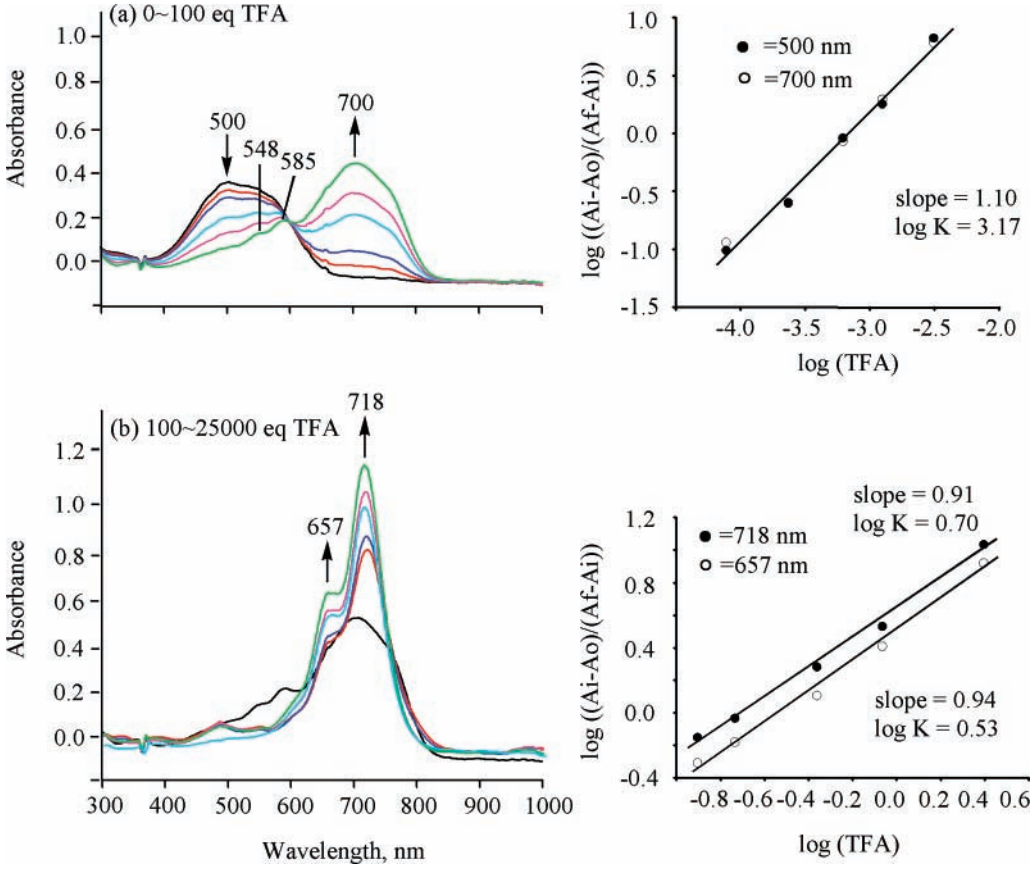

Figure 6. Spectral changes seen upon the addition of TFA to a CH_2Cl_2 solution of $\mathbf{P_4H_2}$, showing the conversion to (a) $\mathbf{P_4H_3}^+$ upon the addition of ca. 100 equiv acid and to (b) $\mathbf{P_4H_4}^{2+}$ after the addition of further TFA (up. to ca. 25 000 equiv).

SCHEME 2

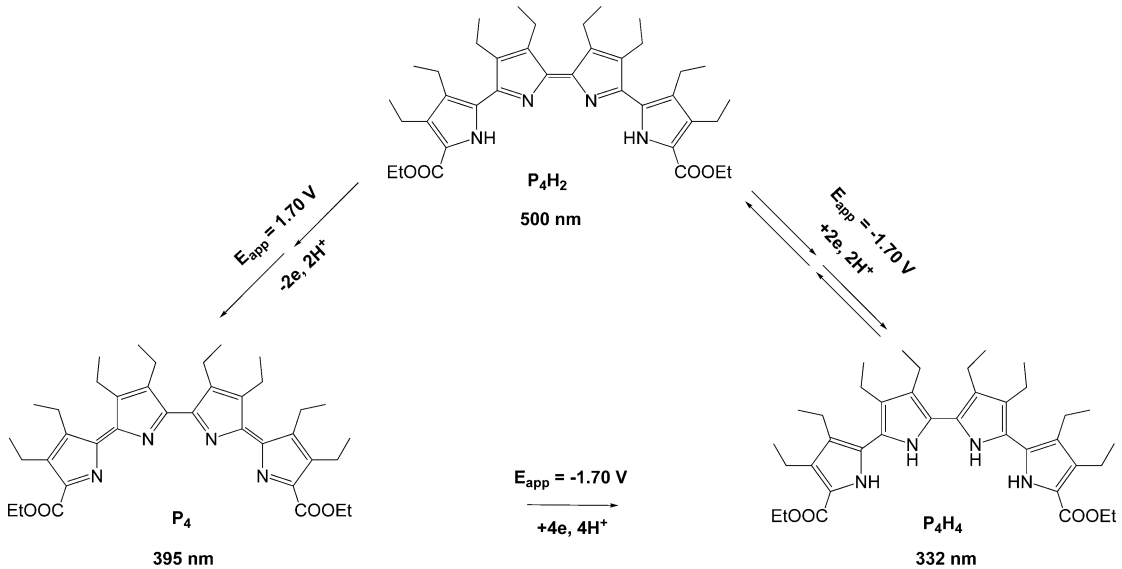

initial electrochemical oxidation of $\mathbf{P_4H_2}$ and is characterized by a major band at 700 nm, a shoulder at 761 nm, and two smaller bands at 548 and 585 nm (Figure 6a). On the basis of the slope of this line (slope = 1.10), the resulting spectrum was assigned to $\mathbf{P_4H_3}^{3+}$. New spectral features are observed after the addition of between 100 and 25000 equiv of TFA. In particular, two major bands are seen at 657 and 718 nm after such additions. These features are similar to those seen in the spectrum recorded after $\mathbf{P_4H_2}$ is subject to a second electrochemical oxidation (Figure 2c). On the basis of this analogy, we conclude that the final protonation product produced from $\mathbf{P_4H_2}$ is $\mathbf{P_4H_4}^{2+}$.

On the basis of the results of the electrochemical and chemical oxidation studies, as well as the protonation experiments described above, a proposed mechanism for the oxidation of $\mathbf{P_4H_2}$ in CH_2Cl_2 was derived; it is shown in Scheme 3.

Key features of this mechanism are that the first one-electron oxidation of $\mathbf{P_4H_2}$ results in the formation of $\mathbf{P_4H_2}^{\bullet+}$, a species that is readily deprotonated to produce $\mathbf{P_4H}^{\bullet}$. This radical intermediate then disproportionates to yield $\mathbf{P_4H_2}$ and $\mathbf{P_4}$. The

SCHEME 3

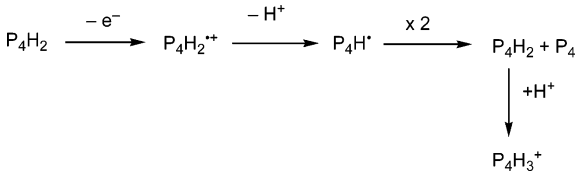

P_4H_2 produced by this process is then protonated by the proton released from **$P_4H_2^{\bullet+}$** to give **$P_4H_3^+$**, a species whose spectrum is characterized by a band at 700 nm, a shoulder at 760 nm, and two smaller bands at 548 and 595 nm.

The second oxidation of **P_4H_2** at $E_{app} = +1.30$ V results, after 300 s, in a shift of the absorption band at 700 to 718 nm. The same type of spectral changes are observed during the titration of **P_4H_2** with TFA at higher acid concentrations (see Figure 6b). Such a congruence leads us to attribute the absorption band at 718 nm to the formation of the same doubly protonated species, **$P_4H_4^{2+}$**, that is formed upon protonation of **$P_4H_3^+$**.

At the relatively high electrode potential of 1.70 V vs SCE, even the doubly protonated species, **$P_4H_4^{2+}$**, can be oxidized. This gives rise to the four electron oxidized form of the quaterpyrrole **P_4** (two electron oxidized relative to **P_4H_2**), a species that has no absorption bands in the 500−1000 nm region ($\lambda_{max} = 395$ nm).

In the presence of high concentrations of TFA, conditions under which **P_4H_2** is converted to **$P_4H_4^{2+}$**, the electrochemical

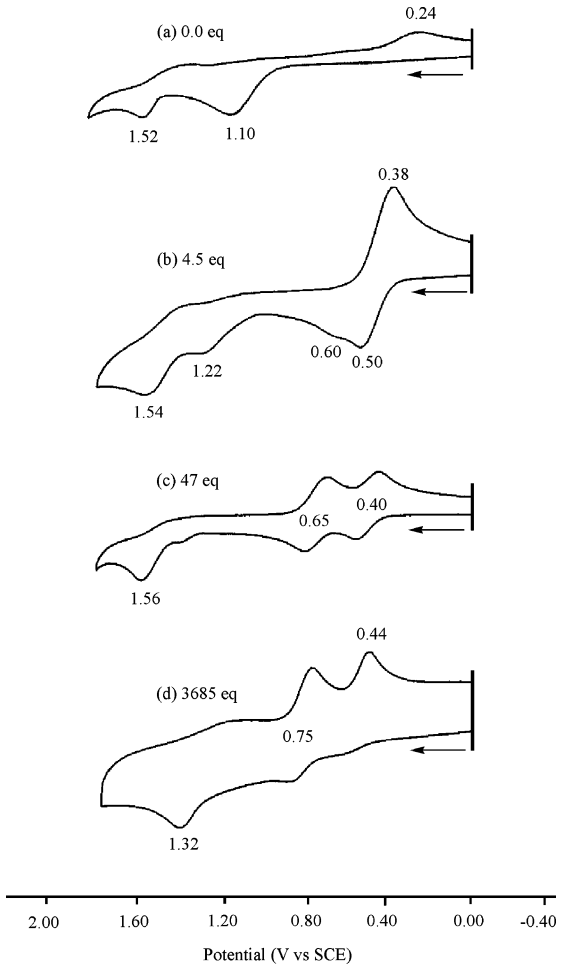

Figure 7. Cyclic voltammograms of **P_4H_2** recorded in CH_2Cl_2 containing 0.1 M TBAP in the presence of 0 to ca. 3685 equiv of TFA.

SCHEME 4

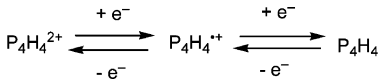

processes become reversible, as can be seen from an inspection of Figure 7. In any case, it is critical to note that the two quasi-reversible electrochemical processes observed for **P_4H_2** in the presence of high concentrations of TFA (where **$P_4H_4^{2+}$** is considered the dominant species) are similar to those seen upon reduction of **P_4H_4**.[13] This is fully consistent with the conclusion that the two quasi-reversible processes in question correspond to two one-electron processes that serve to interconvert **$P_4H_4^{2+}$** with **P_4H_4**, as shown in Scheme 4.

The controlled potential electroreduction of **$P_4H_4^{2+}$** at $E_{app} = 0.70$ V results in the formation of **$P_4H_4^{\bullet+}$**, a species that displays absorption bands (887 and 996 nm) in the near-IR region and is characterized by the absence of an absorption band at 718 nm ascribable to **$P_4H_4^{2+}$** (Figure 8a). The NIR bands due to **$P_4H_4^{\bullet+}$** are significantly red-shifted as compared with those of bipyrrole radical cations (560−600 nm),[15a] due to delocalization of the π electron density over four pyrrole units.[17] At $E_{app} = 0.70$ V, **$P_4H_4^{2+}$** is not oxidized but reduced to give **$P_4H_4^{\bullet+}$**. However, **$P_4H_4^{\bullet+}$** is oxidized back to **$P_4H_4^{2+}$** upon changing the applied potential from 0.70 to 1.10 V. This disparity, though initially surprising, illustrates the effect that protonation can have on the redox chemistry of quaterpyrrole.

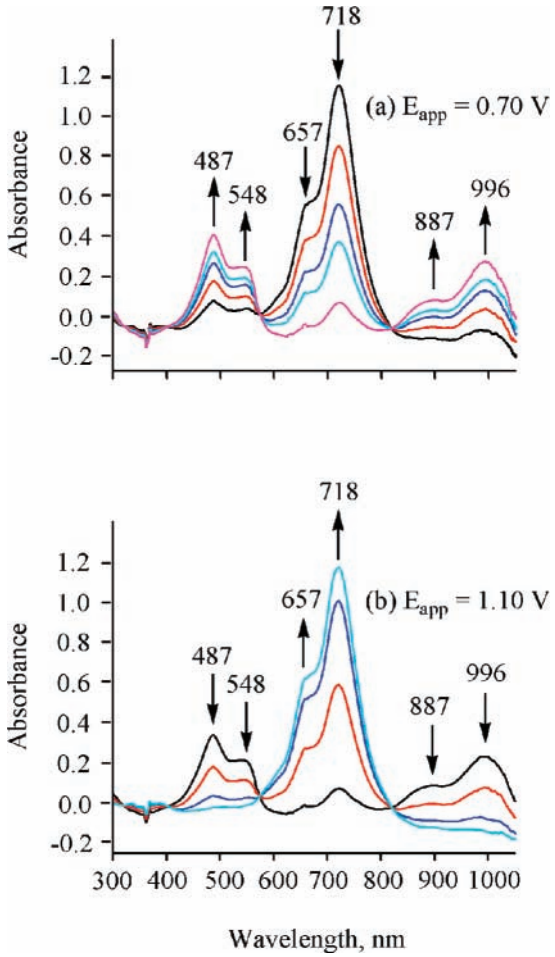

Figure 8. Spectral changes observed when **$P_4H_4^{2+}$** is subject to an electrochemical (a) reduction at $E_{app} = 0.70$ V and (b) reoxidation at 1.10 V vs SCE in CH_2Cl_2 containing 0.2 M TBAP and 600 molar equiv of TFA relative to the quaterpyrrole.

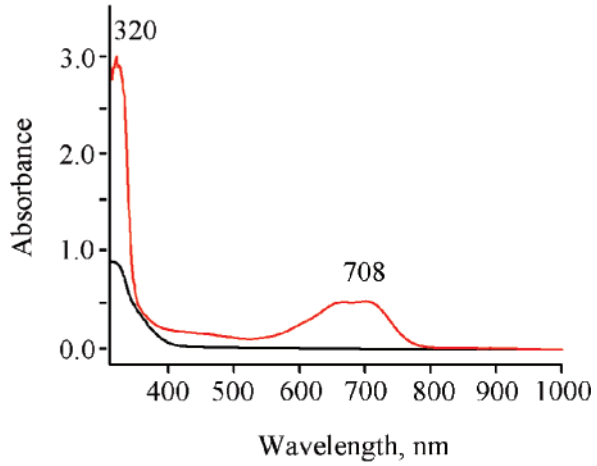

Figure 9. UV−visible spectral changes observed upon the addition tetra-*n*-butylammonium hydroxide (TBAOH) to $\mathbf{P_4H_4}$ in CH_2Cl_2. Black line: Spectrum recorded in the absence of TBAOH. Red line: Spectrum recorded after the addition of ca. 1 equiv of TBAOH.

SCHEME 5

$$P_4H_2 \xrightarrow{+\,e^-} P_4H_2^{\bullet -} \xrightarrow[x\,2]{+\,H^+} P_4H_2 + P_4H_3^-$$

Deprotonation of $\mathbf{P_4H_4}$ in $\mathbf{CH_2Cl_2}$. To investigate the product of the first one-electron reduction of $\mathbf{P_4H_2}$, a base, tetrabutylammonium hydroxide (TBAOH), was added to a CH_2Cl_2 solution of $\mathbf{P_4H_4}$. Under these conditions, a spectrum similar to that produced during the first reduction of $\mathbf{P_4H_2}$ was obtained as shown in Figure 9. It is thus concluded that deprotonation of $\mathbf{P_4H_4}$ results in formation of $\mathbf{P_4H_3}^-$, a species that is characterized by absorption bands at 320 and 708 nm.

On the basis of the above findings, the reduction chemistry of $\mathbf{P_4H_2}$ can be summarized as shown in Scheme 5. The first reduction results in formation of $\mathbf{P_4H_2}^{\bullet -}$, a species that disproportionates to yield $\mathbf{P_4H_2}$ and $\mathbf{P_4H_3}^-$. The disproportionation reaction in Scheme 5 could be directly monitored by laser flash photolysis measurements for the photoinduced electron-transfer reduction of $\mathbf{P_4H_2}$, as described in later sections of the manuscript. As a result of these follow-up reactions, the first cathodic peak seen in Figure 1 is irreversible.

The second one-electron reduction of $\mathbf{P_4H_2}$ at $E_{app} = -1.35$ V (Figure 3b) produces little change in the absorption band at 332 nm (position or intensity). However, the band at 708 nm band essentially disappears. As a result, the final UV−visible spectrum, recorded at the completion of electrolysis, is virtually identical to that of $\mathbf{P_4H_4}$ produced by chemical means,[16,17] at least when the spectrum of the latter product is recorded under conditions identical to those used for the electrochemical analyses (Figure 3b). In this context, it is important to note that the reduced quaterpyrrole species, $\mathbf{P_4H_4}$, displays few absorption features in the visible region, whereas the oxidized species, $\mathbf{P_4H_2}$, is characterized by a broad band centered around 500 nm (ϵ, M^{-1} cm^{-1} = 37 900).[17]

ESR Spectra of Radical Anion and Radical Cation of $\mathbf{P_4H_2}$. The presumed radical anion intermediate produced during the two-electron reduction of $\mathbf{P_4H_2}$ to $\mathbf{P_4H_4}$ was examined by ESR methods. For these latter analyses, the putative radical anion of $\mathbf{P_4H_2}$ was produced by photoinduced electron transfer from dimeric 1-benzyl-1,4-dihydronicotinamide, $(BNA)_2$,[20] to $\mathbf{P_4H_2}$ in dichloromethane (CH_2Cl_2) as shown in Scheme 6. Although the temperature (193 K) and reductant obviously differ from those employed for the electrochemical analyses (factors

SCHEME 6

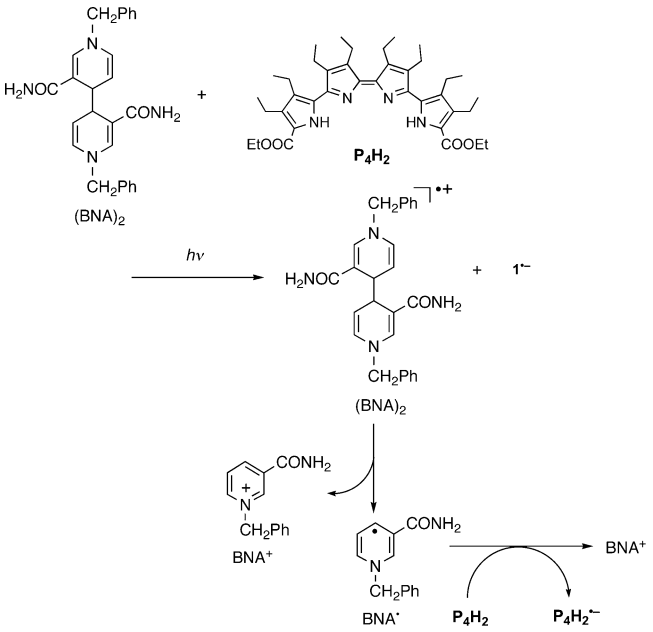

dictated by experimental considerations), it was believed to produce an analogous intermediate. In fact, photoinduced electron transfer from the excited state of $(BNA)_2$ to $\mathbf{P_4H_2}$ is thought to produce both $(BNA)_2^{\bullet +}$ and $\mathbf{P_4H_2}^{\bullet -}$, an initial reaction that was expected to be followed by facile C−C bond cleavage of $(BNA)_2^{\bullet +}$ to produce $BNA^{\bullet}$ and BNA^+.[20] Because the oxidation potential of $BNA^{\bullet}$ (−1.1 V)[24] is more negative than the oxidation peak potential of $\mathbf{P_4H_2}$ (Figure 1), electron transfer from $BNA^{\bullet}$ to $\mathbf{P_4H_2}$ was expected to occur efficiently to produce BNA^+ and $\mathbf{P_4H_2}^{\bullet -}$. Thus, $(BNA)_2$ should act as a unique two-electron donor to produce two equivalents of the radical anion $\mathbf{P_4H_2}^{\bullet -}$ (Scheme 6).[20] Although $\mathbf{P_4H_2}^{\bullet -}$ is not stable on the CV time scale at 298 K as indicated by the irreversible nature of the oxidation peak of $\mathbf{P_4H_2}$ (seen in Figure 1), photoirradiation of a CH_2Cl_2 solution of $\mathbf{P_4H_2}$ and $(BNA)_2$ at a low temperature (193 K) allows the ESR spectrum of $\mathbf{P_4H_2}^{\bullet -}$ to be detected under the steady-state conditions as shown in Figure 10a. The *g* value of $\mathbf{P_4H_2}^{\bullet -}$ is determined as 2.0036. This is larger than the free spin value (2.0023). Such a finding is consistent with spin−orbit coupling due to electron spin at the nitrogen atoms, which often display large spin−orbit coupling constants.[25] The hyperfine splitting is not well resolved. However, the observed ESR spectrum is consistent with the computer simulated spectrum obtained by using the hyperfine coupling constants (hfc) predicted by DFT calculations[22] (Figure 10a). The broadening of the ESR signal is consistent with fast electron exchange between $\mathbf{P_4H_2}^{\bullet -}$ and $\mathbf{P_4H_2}$.[26−28]

The radical cation $\mathbf{P_4H_2}^{\bullet +}$ was produced by treating $\mathbf{P_4H_2}$ with $[Ru(bpy)_3]^{3+}$ (bpy = 2,2′-bipyridine) in acetonitrile. This choice of solvent was dictated by solubility considerations, whereas the choice of oxidant reflected the need for a one electron-transfer species with a potential positive enough to effect the desired oxidation. The oxidation potential of $[Ru(bpy)_3]^{3+}$ is 1.24 V vs SCE in acetonitrile,[29] which, on the basis of the electrochemical analyses carried out in dichloromethane (an admittedly different solvent), was considered positive enough to oxidize $\mathbf{P_4H_2}$. Although $\mathbf{P_4H_2}^{\bullet +}$ is unstable at 298 K in dichloromethane, as inferred from the irreversible oxidation peak in Figure 1, the ESR spectrum of $\mathbf{P_4H_2}^{\bullet +}$ could be observed at a low temperature (253 K), as shown in Figure 4b. The *g* value (2.0032) is larger than the free spin value (2.0023), from which

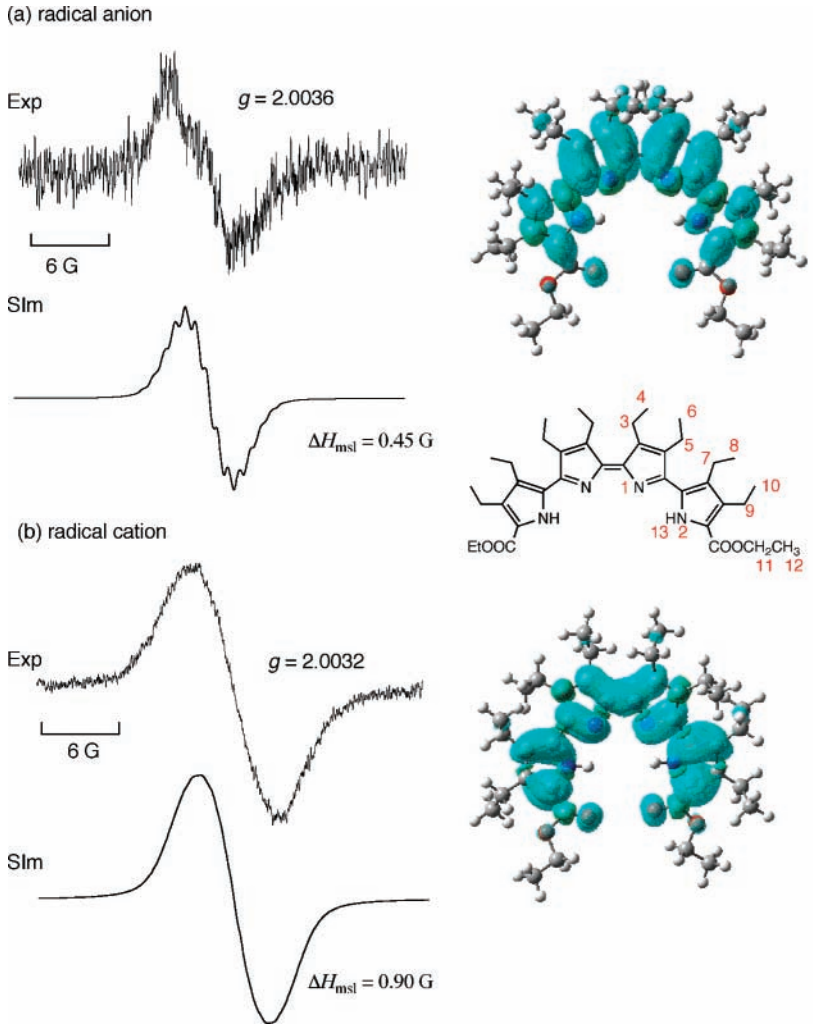

		hfc (G)	
		Exp	DFT
1	2N	0.70	0.66
2	2N	0.70	0.72
3	4H	1.00	1.03
4	6H	-	0.09
5	4H	-	0.45
6	6H	-	0.09
7	4H	-	0.50
8	6H	-	0.01
9	4H	-	0.24
10	6H	-	0.01
11	4H	-	0.16
12	6H	-	0.01
13	2H	0.85	0.85

		hfc (G)	
		Exp	DFT
1	2N	1.56	1.56
2	2N	0.63	0.63
3	4H	-	0.26
4	6H	-	0.01
5	4H	0.65	0.62
6	6H	-	0.03
7	4H	0.65	0.68
8	6H	-	0.04
9	4H	-	0.14
10	6H	-	0.09
11	4H	-	0.36
12	6H	-	0.01
13	2H	-	0.12

Figure 10. (a) ESR spectrum of $\mathbf{P_4H_2}^{\bullet-}$ produced by the photoinduced electron transfer from $(BNA)_2$ (5.0×10^{-3} M) to $\mathbf{P_4H_2}$ (2.0×10^{-4} M) in CH_2Cl_2 at 193 K and the corresponding computer simulated spectrum. (b) ESR spectrum of $\mathbf{P_4H_2}^{\bullet+}$ produced by the electron-transfer oxidation of $\mathbf{P_4H_2}$ (3.0×10^{-5} M) with $[Ru(bpy)_3]^{3+}$ (3.0×10^{-5} M) in MeCN at 253 K with the computer simulation spectrum. The computer simulation spectra of $\mathbf{P_4H_2}^{\bullet-}$ and $\mathbf{P_4H_2}^{\bullet+}$ are obtained using the hfc values predicted by DFT calculations in the Tables.

SCHEME 7

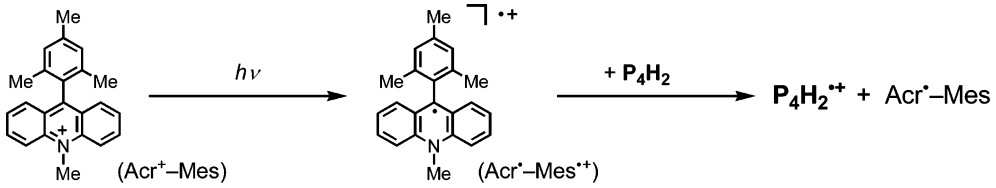

we conclude that spin−orbit coupling from the nitrogen atoms is also important in this case.[25] The observed ESR spectrum is again consistent with the computer simulated spectrum obtained as above (Figure 10). In contrast with the ESR spectrum reported previously for the radical cation of bipyrrole, a species that exhibited a well-resolved hyperfine structure,[17] no hyperfine structure was observed for $\mathbf{P_4H_2}^{\bullet+}$.

The one-electron oxidized form of $\mathbf{P_4H_4}$, specifically the radical cation $\mathbf{P_4H_4}^{\bullet+}$, was produced by treating $\mathbf{P_4H_4}$ with $[Ru(bpy)_3]^{3+}$ as above. Again, a broader ESR spectrum was observed for this species than for the corresponding bipyrrole-derived species.[17] On the basis of this disparity, we conclude that increasing the extent to which the unpaired electron is delocalized (over up to four, as opposed to two pyrrolic subunits) leads to a greater rate of electron exchange, which in the case of $\mathbf{P_4H_4}^{\bullet+}$ is manifest in terms of a broader spectrum and a lower level of hyperfine structure.[28]

Laser Flash Photolysis. Nanosecond laser flash photolysis was used to elucidate the mechanistic details. Transient absorption spectra taken after the nanosecond laser excitation at 355 nm of a deaerated MeCN solution of $(BNA)_2$ in the presence of $\mathbf{P_4H_2}$ are shown in Figure 11. Note that the transient absorption band is observed at 25 μs after laser excitation (black line in Figure 11a). The absorption band at 700 nm that then appears at 800 μs (red line in Figure 11a), is assigned by $\mathbf{P_4H_3}^{-}$, on the basis of its congruence with the one for $\mathbf{P_4H_3}^{-}$ recorded following the electrochemical reduction of $\mathbf{P_4H_2}$. The negative absorption around 530 nm is due to the bleaching of the absorption for $\mathbf{P_4H_2}$. The increase in intensity at 700 nm coincides with the increase in the bleaching at 530 nm, and

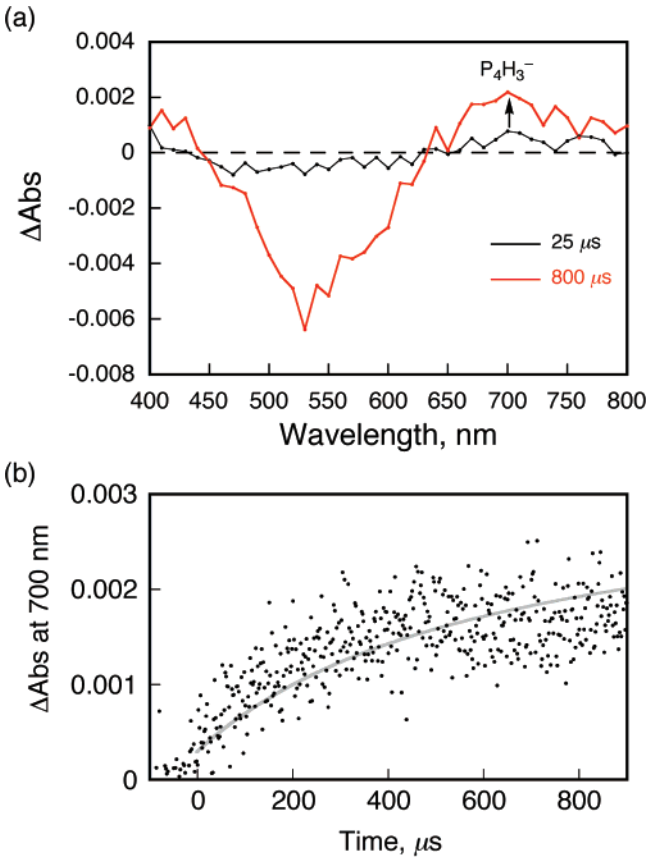

Figure 11. (a) Nanosecond transient absorption spectra obtained from photoinduced electron transfer from $(BNA)_2$ (5.0×10^{-4} M) to $\mathbf{P_4H_2}$ (3.0×10^{-4} M) in MeCN after irradiation by the 355 nm laser pulse at the indicated time intervals at 298 K. (b) Time profile at 700 nm. The gray line represents the best fit to second-order kinetics.

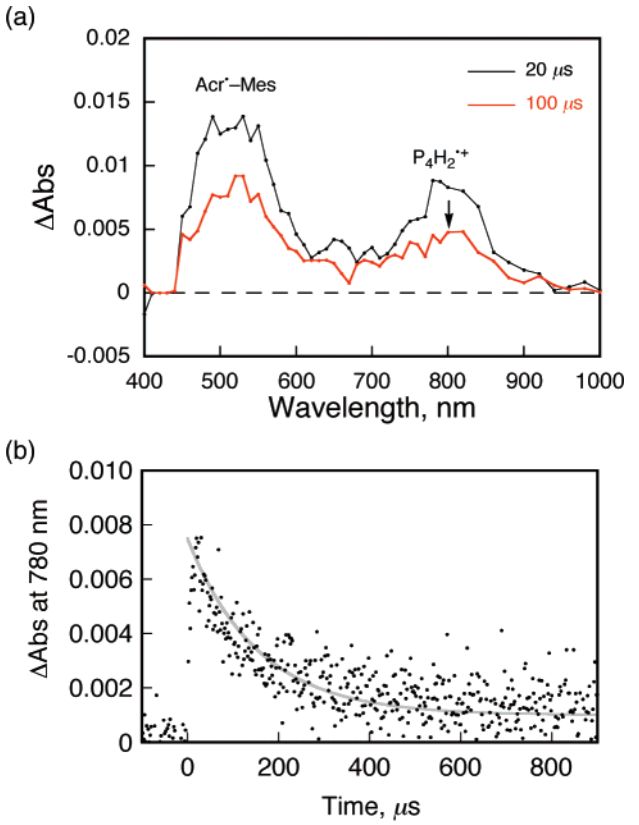

Figure 12. (a) Nanosecond transient absorption spectra of $\mathbf{P_4H_2}^{\bullet+}$ obtained when $\mathbf{P_4H_2}$ (3.0×10^{-4} M) is subject to photoirradiation in the presence of Acr^+-Mes (1.0×10^{-4} M) in MeCN. Irradiation was effected using a 355 nm laser pulse and the spectra were recorded at 298 K at the indicated time intervals. (b) Time profile at 780 nm. The gray line represents the best fit to a first-order decay process.

both time profiles obey second-order kinetics (see the fitted second-order kinetic line shown as the inset to Figure 11b). The rate constant for this increase was determined to be 2.1×10^{10} M^{-1} s^{-1}, which is close to the diffusion-controlled rate in MeCN (2.0×10^{10} M^{-1} s^{-1}).[30] These results thus provide support for the conclusion that $\mathbf{P_4H_3}^-$ is formed via disproportionation of $\mathbf{P_4H_2}^{\bullet-}$, a species that, in turn, is generated by electron trasnfer from $(BNA)_2$ to $\mathbf{P_4H_2}$ (Scheme 5).[31]

To complement the above studies, nanosecond laser flash photolysis experiments were carried out in the presence of the 9-mesityl-10-methylacridinium ion (Acr^+-Mes).[32,33] Photoirradiation of Acr^+-Mes gives a long-lived electron-transfer state, which can act as an oxidant for $\mathbf{P_4H_2}$. In the event, nanosecond laser excitation at 355 nm of a deaerated MeCN solution of Acr^+-Mes results in formation of the electron-transfer state ($Acr^{\bullet}-Mes^{\bullet+}$), presumably as the result of photoinduced electron transfer from the mesitylene moiety to the singlet excited state of acridinium moiety (Scheme 7).

Because the one-electron reduction potential of $Acr^{\bullet}-Mes^{\bullet+}$ ($E_{red} = 1.88$ V vs SCE) is more positive than the one-electron oxidation potential of $\mathbf{P_4H_2}$, electron transfer from $\mathbf{P_4H_2}$ to $Acr^{\bullet}-Mes^{\bullet+}$ is energetically feasible. Thus, the addition of $\mathbf{P_4H_2}$ to an MeCN solution of Acr^+-Mes followed by laser photoirradiation results in the formation of $\mathbf{P_4H_2}^{\bullet+}$ ($\lambda_{max} = 780$ nm) and $Acr^{\bullet}-Mes$ ($\lambda_{max} = 520$ nm),[32,33] as shown in Figure 12a. The decay of the $\mathbf{P_4H_2}^{\bullet+}$ intermediate produced in this way obeys first-order kinetics (Figure 12b) independent of laser power intensity (5−20 mJ/pulse), with the corresponding rate constant being 6.5×10^3 s^{-1}. We thus conclude that the rate-determining step is deprotonation of $\mathbf{P_4H_2}^{\bullet+}$ to produce $\mathbf{P_4H}^{\bullet}$ as an intermediate (Scheme 3).

Conclusions

We have demonstrated that the oxidized form of a quaterpyrrole ($\mathbf{P_4H_2}$) exhibits electron-transfer properties that are analogous to those seen for porphyrins. In particular, $\mathbf{P_4H_2}$ is susceptible to both facile multiple-electron oxidations and reductions. Both the singly oxidized ($\mathbf{P_4H_2}^{\bullet+}$) and singly reduced species ($\mathbf{P_4H_2}^{\bullet-}$) have been successfully detected by ESR, showing spin delocalization over the four pyrrole units in both cases. The rates of deprotonation from $\mathbf{P_4H_2}^{\bullet+}$ and disproportionation of $\mathbf{P_4H_2}^{\bullet-}$ were determined by laser flash photolysis measurements of the photoinduced electron-transfer oxidation and reduction of $\mathbf{P_4H_2}$, respectively. Thus, quaterpyrrole in its various oxidized/reduced forms can be regarded as a rudimentary electronic model for porphyrins.

Acknowledgment. The support of the National Science Foundation (grant CHE-0515670 to J.L.S.), the Robert A. Welch Foundation (Grants E-680 and F-1018 to K.M.K. and J.L.S., respectively) and a Grant-in-Aid (Nos. 19205019 and 19750034 to S.F. and K.O.) from the Ministry of Education, Culture, Sports, Science and Technology, Japan, is gratefully acknowledged.

References and Notes

(1) Guernion, N. J. L.; Hayes, W. *Curr. Org. Chem.* **2004**, *8*, 637.
(2) (a) Sessler, J. L.; Weghorn, S. J. In *Expanded, Contracted and Isomeric Porphyrins*, Elsevier: Oxford, U.K., 1997. (b) Sessler, J. L.;

Gebauer, A.; Weghorn, S. J. In *Porphyrin Handbook*; Kadish, K. M., Smith, K. M., Guilard, R., Eds.; Academic Press: San Diego 1999; Vol. 2, Chapter 9.

(3) Sessler, J. L.; Seidel, D. *Angew. Chem., Int. Ed.* **2003**, *42*, 5134.

(4) Chandrashekar, T. K.; Venkatraman, S. *Acc. Chem. Res.* **2003**, *36*, 676.

(5) Lash, T. D. *Chem. Eur. J.* **1996**, *2*, 1197.

(6) Chou, J. H.; Nalwa, H. S.; Kosal, M. E.; Rakow, N. A.; Suslick, K. S. In *Porphyrin Handbook*; Kadish, K. M., Smith, K. M., Guilard, R., Eds.; Academic Press: San Diego, 1999; Vol. 6, Chapter 41.

(7) Pandey, R. K.; Zheng, G. In *Porphyrin Handbook*; Kadish, K. M., Smith, K. M., Guilard, R., Eds.; Academic Press: San Diego, 1999; Vol. 6, Chapter 43.

(8) (a) Rapoport, H.; Castagnoli, N. *J. Am. Chem. Soc.* **1962**, *84*, 2178. (b) Bordner, J.; Rapoport, H. *J. Org. Chem.* **1965**, *30*, 3824.

(9) (a) Grigg, R.; Johnson, A. W.; Wasley, J. W. F. *J. Chem. Soc.* **1963**, 359. (b) Bauer, V. J.; Clive, D. L. J.; Dolphin, D.; Paine, J. B., III; Harris, F. L.; King, M. M.; Loder, J.; Wang, S. W. C.; Woodward, R. B. *J. Am. Chem. Soc.* **1983**, *105*, 6429.

(10) Ikeda, H.; Sessler, J. L. *J. Org. Chem.* **1993**, *58*, 2340.

(11) Sessler, J. L.; Weghorn, S. J.; Hiseada, Y.; Lynch, V. *Chem. Eur. J.* **1995**, *1*, 56.

(12) Iyoda, M.; Otsuka, H.; Sato, K.; Nisato, N.; Oda, M. *Bull. Chem. Soc. Jpn.* **1990**, *63*, 80.

(13) (a) Groenendaal, L.; Peerlings, H. W. I.; Havinga, E. E.; Vekemans, J. A. J. M.; Meijer, E. W. *Synth. Met.* **1995**, *69*, 467. (b) Martina, S.; Enkelmann, V.; Schluter, A. D.; Wegner, G. *Synth. Met.* **1991**, *41*, 403.

(14) Sessler, J. L.; Seidel, D.; Vivian, A. E.; Lynch, V.; Scott, B. L.; Keogh, D. W. *Angew. Chem. Int. Ed.* **2001**, *40*, 591.

(15) Detailed investigations have so far been made only for the electronic, electrochemical, and spectroscopic properties of bipyrroles; see: (a) Guyard, L.; Hapiot, P.; Neta, P. *J. Phys. Chem. B* **1997**, *101*, 5698. (b) Guyard, L.; Hapiot, P.; Jouini, M.; Lacroix, J.-C.; Lagrost, C.; Neta, P. *J. Phys. Chem. A* **1999**, *103*, 4009.

(16) Sessler, J. L.; Aguilar, A.; Sanchez-Garcia, D.; Seidel, D.; Köhler, T.; Arp, F.; Lynch, V. M. *Org. Lett.* **2005**, *7*, 1887.

(17) E, W.; Ohkubo, K.; Sanchez-Garcia, D.; Zhang, M.; Sessler, J. L.; Fukuzumi, S.; Kadish, K. M. *J. Phys. Chem B* **2007**, *111*, 4320.

(18) Kadish, K. M.; van Caemelbecke, E.; Royal, G. In *Porphyrin Handbook*; Kadish, K. M., Smith, K. M., Guilard, R., Eds.; Academic Press: San Diego, 2000; Vol. 8, pp 1−114.

(19) Wallenfels, K.; Gellerich, M. *Chem. Ber.* **1959**, *92*, 1406.

(20) (a) Patz, M.; Kuwahara, Y.; Suenobu, T.; Fukuzumi, S. *Chem. Lett.* **1997**, 567. (b) Fukuzumi, S.; Suenobu, T.; Patz, M.; Hirasaka, T.; Itoh, S.; Fujitsuka, M.; Ito, O. *J. Am. Chem. Soc.* **1998**, *120*, 8060.

(21) Lin, X. Q.; Kadish, K. M. *Anal. Chem.* **1985**, *57*, 1498.

(22) (a) Becke, A. D.; *J. Chem. Phys.* **1993**, *98*, 5648. (b) Lee, C.; Yang, W.; Parr, R. G. *Phys. Rev. B* **1988**, *37*, 785.

(23) Frisch, M. J.; Trucks, G. W.; Schlegel, H. B.; Scuseria, G. E.; Robb, M. A.; Cheeseman, J. R.; Montgomery, J. A., Jr.; Vreven, J. T.; Kudin, K. N.; Burant, J. C.; Millam, J. M.; Iyengar, S. S.; Tomasi, J.; Barone, V.; Mennucci, B.; Cossi, M.; Scalmani, G.; Rega, N.; Petersson, G. A.; Nakatsuji, H.; Hada, M.; Ehara, M.; Toyota, K.; Fukuda, R.; Hasegawa, J.; Ishida, M.; Nakajima, T.; Honda, Y.; Kitao, O.; Nakai, H.; Klene, M.; Li, X.; Knox, J. E.; Hratchian, H. P.; Cross, J. B.; Adamo, C.; Jaramillo, J.; Gomperts, R.; Stratmann, R. E.; Yazyev, O.; Austin, A. J.; Cammi, R.; Pomelli, C.; Ochterski, J. W.; Ayala, P. Y.; Morokuma, K.; Voth, G. A.; Salvador, P.; Dannenberg, J. J.; Zakrzewski, V. G.; Dapprich, S.; Daniels, A. D.; Strain, M. C.; Farkas, O.; Malick, D. K.; Rabuck, A. D.; Raghavachari, K.; Foresman, J. B.; Ortiz, J. V.; Cui, Q.; Baboul, A. G.; Clifford, S.; Cioslowski, J.; Stefanov, B. B.; Liu, G.; Liashenko, A.; Piskorz, P.; Komaromi, I.; Martin, R. L.; Fox, D. J.; Keith, T.; Al-Laham, M. A.; Peng, C. Y.; Nanayakkara, A.; Challacombe, M.; Gill, P. M. W.; Johnson, B.; Chen, W.; Wong, M. W.; Gonzalez, C.; Pople, J. A. *Gaussian 03 Revision C.02*; Gaussian, Inc.: Wallingford, CT, 2004.

(24) Fukuzumi, S.; Koumitsu, S.; Hironaka, K.; Tanaka, T. *J. Am. Chem. Soc.* **1987**, *109*, 305.

(25) Wertz, J. E.; Bolton J. R. *Electron Spin Resonance Elementary Theory and Practical Applications*; McGraw-Hill Book Co.: New York, 1972.

(26) Fukuzumi, S.; Endo, Y.; Imahori, H. *J. Am. Chem. Soc.* **2002**, *124*, 10974.

(27) Cheng, K. S.; Hirota, N. In *Investigation of Rates and Mechanisms of Reactions*; Hammes, G. G., Ed.; Wiley-Interscience: New York, 1974; Vol. *VI*, pp 565.

(28) Fukuzumi, S.; Hasobe, T.; Endo, Y.; Ohkubo, K.; Imahori, H. *J. Porphyrins Phthalocyanines* **2003**, *7*, 328.

(29) Fukuzumi, S.; Nakanishi, I.; Tanaka, K.; Suenobu, T.; Tabard, A.; Guilard, R.; Van Caemelbecke, E.; Kadish, K. M. *J. Am. Chem. Soc.* **1999**, *121*, 785.

(30) Rehm, A.; Weller, A. *Isr. J. Chem.* **1970**, *8*, 259.

(31) The transient absorption due to $\mathbf{P_4H_2}^{\bullet-}$ was not observed probably because of the low extinction coefficient.

(32) (a) Fukuzumi, S.; Kotani, H.; Ohkubo, K.; Ogo, S.; Tkachenko, N. V.; Lemmetyinen, H. *J. Am. Chem. Soc.* **2004**, *126*, 1600. (b) Ohkubo, K.; Kotani, H.; Fukuzumi, S. *Chem. Commun.* **2005**, 4520.

(33) Kotani, H.; Ohkubo, K.; Fukuzumi, S. *J. Am. Chem. Soc.* **2004**, *126*, 15999.